ARTICLE

Effect of Homogenization Rates on the Properties and Stability of Fish Gelatin Films with Cinnamon Essential Oil

See Cheng Lee[1], Han Lyn Foong[1] and Nur Hanani Z. A.[1,2,*]

[1]Department of Food Technology, Faculty of Food Science and Technology, Universiti Putra Malaysia, Serdang, 43400, Malaysia

[2]Institute of Tropical Forestry and Forest Products, Universiti Putra Malaysia, Serdang, 43400, Malaysia

*Corresponding Author: Nur Hanani Z. A. Email: hanani@upm.edu.my

ABSTRACT

Fish gelatin films have emerged as eco-friendly packaging materials due to their biodegradability and excellent film-forming properties. This study investigated the effects of varying homogenization rates (0, 6500, 9500, 13,500, 17,500, and 21,500 rpm) on the functional and structural properties of fish gelatin films enriched with cinnamon essential oil (CEO). Homogenization reduced droplet sizes and narrowed droplet size distributions in the film-forming emulsion (FFE). At a homogenization rate of 9500 rpm, the films exhibited excellent mechanical extensibility, reduced surface irregularities, and enhanced smoothness. The highest ($p < 0.05$) tensile strength and elongation at break were observed at this rate, showing increases of 57% and 14%, respectively, compared to the control film made from non-homogenized FFE. However, further increases in homogenization rates significantly increased ($p < 0.05$) water vapor permeability and caused CEO droplets aggregation, leading to increased surface irregularities and the formation of pores in the film microstructure. These structural changes were observed through confocal laser scanning microscopy (CLSM), scanning electron microscopy (SEM), and atomic force microscopy (AFM). These findings indicate that the film properties were significantly influenced by the homogenization rate, highlighting its role in tailoring the mechanical and barrier properties of fish gelatin/CEO films for food packaging applications.

KEYWORDS

Homogenization rate; cinnamon essential oil; fish gelatin film; biodegradable packaging; functional properties

Nomenclature

AFM	Atomic force microscopy
CEO	Cinnamon essential oil
CLSM	Confocal laser scanning microscopy
FFE	Film-forming emulsion
RH	Relative humidity
SEM	Scanning electron microscopy

1 Introduction

Biodegradable polymers are increasingly studied as alternatives to conventional plastic due to their environmental benefits. Traditional petrochemical-based plastics are estimated to contribute approximately 15% of global carbon emissions, equivalent to around 1.7 gigatons of CO_2 [1]. In contrast, biodegradable polymers can be derived from renewable sources such as agricultural feedstocks, marine industry by-products, animal, and microbial sources [2,3]. Common biopolymers used in packaging films include polysaccharides, lipids, and proteins, which may be combined to enhance their functional and mechanical properties [4].

Fish gelatin is a protein-based biopolymer and is extracted from the collagen in fish bones and skin. As food packaging, it is valued for its film-forming ability, biodegradability, biocompatibility, and excellent barrier properties against gases, volatile compounds, oils, and UV light [1,5–7]. Additionally, fish gelatin is a sustainable choice that aligns with religious and cultural dietary restrictions, avoiding health and ethical concerns linked to porcine and bovine sources [8]. Despite its benefits, fish gelatin has several limitations that must be addressed for broader application in food packaging. Pure gelatin films are typically brittle and are prone to cracking due to disulfide bonds, hydrogen bonds, and electrostatic interactions that decrease flexibility [9]. Secondly, its hydrophilic nature results in poor water vapor barrier and mechanical properties [10], particularly in high-humidity environments, limiting its application in food packaging [1,11]. To overcome this limitation, essential oils can be incorporated into gelatin to lower its hydrophilicity while improving its antimicrobial and antioxidant properties [12–14].

Essential oils are plant-based secondary metabolites which are approved by the Food and Drug Administration (FDA) as safe biological additives [8]. Due to the abundant bioactive compounds that are present in essential oils, especially those from aromatic spices such as cinnamon [15–17], clove [18,19], and oregano [20,21], they are known for their antimicrobial properties and are used to extend the shelf life of food products [22]. Cinnamon (*Cinnamomum zeylanicum*) essential oil (CEO), a volatile oil commonly obtained from the bark and branches of cinnamon, has been extensively studied for its broad-spectrum antimicrobial activity, including its inhibition of both Gram-positive and Gram-negative bacteria [23–26]. Furthermore, CEO exhibits antioxidant activity due to the bioactive compounds such as cinnamaldehyde, eugenol, and *trans*-cinnamaldehyde [27,28]. Additionally, CEO is categorized as Generally Recognized as Safe (GRAS) by USFDA and is commonly used as an additive in various food products [27]. However, the direct addition of essential oils into food can alter its organoleptic properties.

An alternative approach involves the creation of active packaging, where active compounds such as essential oils are incorporated into the packaging material itself, enhancing the polymer's functional properties [29,30]. Furthermore, using the appropriate concentration of essential oil can mitigate undesirable odors in the films [14]. Previous studies have incorporated CEO into various biobased polymeric films, including polylactic acid [17], zein [31], and poly (butylene adipate-*co*-terephthalate)/ thermoplastic starch composite [26]. In a recent study, Lim et al. [16] demonstrated the effectiveness of poly-ε-caprolactone/CEO films in inhibiting mold growth on bread for up to 21 days.

The process of incorporating essential oils into biobased polymer films or coatings typically involves the creation oil-in-water (O/W) emulsions, in which the oil is dispersed within an aqueous phase and stabilized by an emulsifier [32,33]. The emulsification process is critical to the quality of the resulting film, with droplet size and distribution being key factors [34]. Smaller droplet sizes have been shown to enhance emulsion stability and improve both barrier and mechanical properties. Alharbi et al. demonstrated that the homogenization rate and time significantly influenced droplet size in an emulsion, with smaller droplets (7 μm) exhibiting notably higher stability than larger droplets (27 μm) [35]. This effect is also evident in nanoemulsions. In a study by Chu et al. [36], pullulan films incorporating CEO nanoemulsions with smaller droplets (60 nm) displayed superior water vapor barrier and flexibility compared to those

containing larger CEO droplets (>100 nm). This is because larger oil droplets could create micropores in the film matrix during drying, facilitating moisture transfer [18,21].

One common emulsification method is rotor-stator homogenization, which promotes uniform mixing of lipid and aqueous phases while reducing droplet size. This process relies on the shear forces generated between the rotating rotor and stationary stator to break down lipid droplets, ensuring homogeneous distribution within the film [37]. Previous research has shown that emulsion stability is influenced by factors such as homogenization rate, shearing intensity, pressure, temperature, and time [38,39], with higher homogenization rates producing emulsions with smaller droplets sizes and increased stability [35,39]. However, when the homogenization rate is too high, over-homogenization may occur which can lead to problems such as an increased interfacial tension, increased emulsion viscosity, and denaturation of proteins, and oxidation of thermolabile bioactive compounds [40]. Consequently, the emulsion stability may be affected and coalescence of oil droplets might occur during film drying.

Despite the existing research on emulsification processes, limited studies have explored the effect of homogenization rates on the properties of fish gelatin/CEO film. This study aims to address this gap by investigating how different homogenization rates influence the properties of fish gelatin/CEO films, particularly the barrier and mechanical properties.

2 Materials and Methods

2.1 Materials

Fish gelatin powder (240–260 bloom, 20–40 mesh, gelling temperature, T_{gel} = 25°C) was purchased from Custom Collagen (Addison, IL, USA). Food-grade pure cinnamon essential oil (CEO) from Ceylon cinnamon (*Cinnamomum verum*), steam-distilled with a cinnamaldehyde content of ≥40% and coumarin ≤0.01%, was obtained from Druera (Wilmington, UK). Glycerol was purchased from Sigma-Aldrich (St Louis, MO, USA). Nile Red, Tween 80, and polyethylene glycol were obtained from Acros Organics (Fairlawn, NJ, USA). Fast Green FCF was obtained from Santa Cruz Biotechnology, Inc. (Dallas, TX, USA).

2.2 Preparation of Fish Gelatin/CEO Films

Fish gelatin powder was dissolved in distilled water to achieve a 3.5% (w/v) concentration. The solution was heated at 70°C for 30 min. Glycerol, at 30% (w/w) of the gelatin content, was incorporated as a plasticizer and stirred for another 30 min. These concentrations were selected based on preliminary studies, where a higher gelatin concentration produced overly rigid films, and increased glycerol concentration led to films that became excessively sticky after drying. To prepare the film-forming emulsion (FFE), 0.1% (v/v) CEO, relative to the gelatin solution, was mixed with Tween 80 as an emulsifier, set at 25% (w/w, based on CEO). The CEO concentration was determined based on preliminary studies, as higher concentrations resulted in brittle films. The FFE was homogenized using a rotor-stator homogenizer (Ultra-Turrax T25, IKA Work Inc., Wilmington, DE, USA) at different rates of 6500 rpm (B), 9500 rpm (C), 13,500 rpm (D), 17,500 rpm (E) and 21,500 rpm (F) for 3 min, as shown in Fig. 1. Control films (A) were prepared without homogenization. After homogenization, 20 mL of the FFE was cast onto a petri dish and air-dried at room temperature (25°C ± 2°C) for 48 h. The dried films were manually peeled off and stored at 25°C ± 2°C and 50% ± 5% RH prior to analysis.

2.3 Characterization of Film-Forming Emulsion

The droplet size distribution of the FFE was measured using a laser diffractometer (MasterSizer 2000, Malvern Instruments, Worcestershire, UK). The samples were diluted in distilled water at 2000 rpm until an obstruction rate of 4% was obtained. The Mie theory was applied, considering the following optical property for CEO: a refractive index of 1.57 [41]. Each FFE was measured in triplicate. The surface area-weighted (Sauter) mean diameter (D3,2) and volume-weighted (De Brouckere) mean diameter (D4,3) were determined.

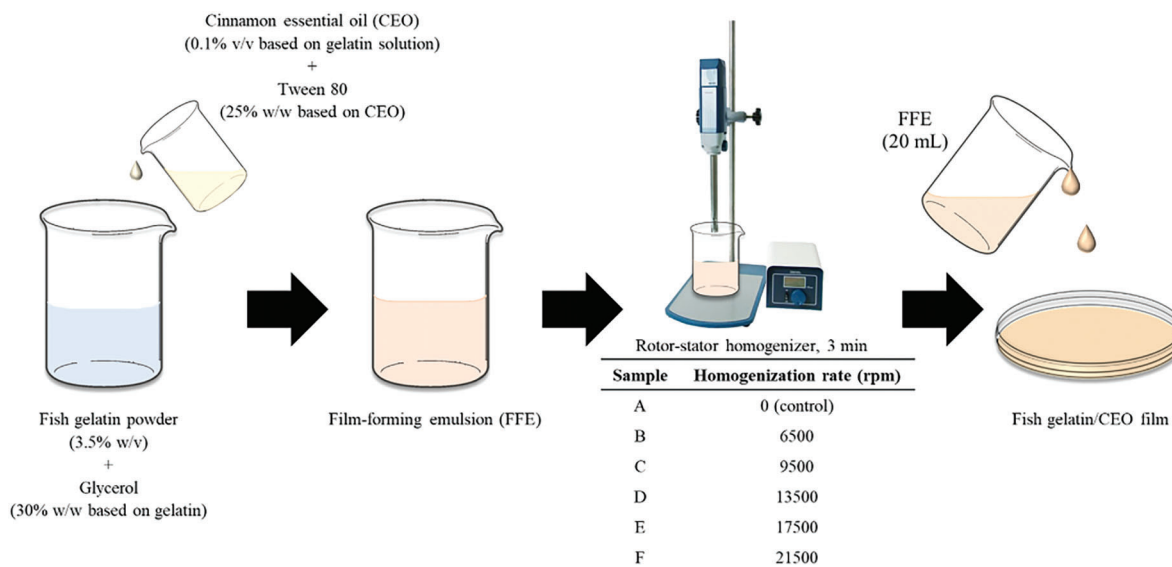**Figure 1:** Preparation of fish gelatin/cinnamon essential oil films

2.4 Film Thickness

The thickness of the film was expressed as the mean thickness at ten random positions on the film, measured using a hand-held digital micrometer (Mitutoyo 547–401 Thickness Gauge, Mitutoyo Co., Kawasaki, Japan).

2.5 Mechanical Properties

The tensile strength (TS) and elongation at break (EAB) of the films were measured using an INSTRON 4302 Series IX Machine (Singapore) equipped with a 10 N tensile load, following the ASTM-D882 standard method [42]. Test films were cut into strips (60 mm × 20 mm) and mounted between two grips with an initial separation of 50 mm. The crosshead speed was set to 100 mm/min.

2.6 Water Vapor Permeability

Water vapor permeability (WVP) of the films was measured according to the ASTM E-96 standard method with slight modifications [43,44]. Distilled water (6 mL) was placed into each test cup, and the film sample was tightly secured over the cup opening. The cups were maintained under controlled temperature and RH (23°C ± 2°C, 50% ± 5% RH). Weight loss from the samples was monitored over a 6-h period, with weights recorded at 1-h intervals. The WVP of the film was then calculated as follows:

$$\text{WVP} \left(\text{g m}^{-1} \text{ Pa}^{-1} \text{ s}^{-1} \right) = \frac{m.x}{A.t.\Delta P} \tag{1}$$

where m = weight loss of the cup (g); x = film thickness (mm); A = area of exposed film (m^2); t = time (s); ΔP = partial vapor pressure difference at 23°C, 2810.06 Pa [45].

2.7 Light Transmittance and Opacity

The percentage of light transmittance was measured at wavelengths of 200, 280, 400, 500, 600, and 800 nm using a UV–Vis spectrophotometer (Thermo Fisher Scientific, Madison, WI, USA). The opacity of the film was calculated as follows:

$$\text{Opacity} \left(\text{AU mm}^{-1} \right) = \frac{Abs_{600}}{x} \tag{2}$$

where Abs_{600} = Absorbance value at 600 nm (AU); x = film thickness (mm).

2.8 Surface Microstructure

The surface microstructure of film samples was visualized using a scanning electron microscope (JSM 6400, JEOL, Akishima, Japan). The samples were mounted on a bronze stub and coated with gold using a sputter coater (SCD 005, BalTec, Canonsburg, PA, USA). All the samples were viewed at a voltage of 15 kV under the magnification of 1000×.

2.9 Confocal Laser Scanning Microscopy

A confocal microscope LSM 5 Pascal Exciter (Zeiss, White Plains, NY, USA) was used to examine the protein phase and oil distribution in the gelatin films, following the method by Auty et al. [46]. Film samples (10 mm × 10 mm) were cut and placed on microscope glass covers, then stained with a 3:1 mixture of 0.02% (w/w) Nile Red in polyethylene glycol and 0.1% (w/w) aqueous Fast Green FCF. Samples were washed with water to remove excess stain before viewing. Fluorescence images were obtained using two separate channels: a Krypton/Argon laser (405 nm excitation) and a Helium/Neon laser (543 nm excitation). Micrographs of the XYZ layer projections were acquired using a 20× objective lens to represent a single image.

2.10 Atomic Force Microscopy

The surface morphology of the films was examined using atomic force microscopy (AFM) with a NanoScope scanning probe microscope (Digital Instruments CP-II, Inc., Santa Barbara, CA, USA). AFM scans were conducted at a scan size of 20 μm × 20 μm, with a vertical range of 5 μm. A three-dimensional surface image (400 μm × 400 μm) was obtained for each sample, with two images recorded per formulation. Two statistical parameters were used to quantify the surface roughness: average roughness (R_a), representing the mean of the absolute height deviations from the average surface level, and root-mean-square roughness (R_q), which calculates the root-mean-square of height deviations from the mean data plane.

2.11 Statistical Analysis

All experiments were conducted in triplicate, and the results are reported as mean ± standard deviation. Statistical analysis was performed using a one-way analysis of variance (ANOVA) with Minitab 16.1 software, at a significance level of 0.05. Post-hoc comparisons were made using the Tukey's test.

3 Results and Discussions

3.1 Characterization of Film-Forming Emulsion

The $D_{3,2}$ and $D_{4,3}$ values of the FFE are shown in Table 1. The FFE for control (A) exhibited $D_{3,2}$ and $D_{4,3}$ values of 4.00 and 5.89 μm, respectively. The larger $D_{4,3}$ value compared to $D_{3,2}$ suggests a notable presence of larger droplets within the FFE, as $D_{4,3}$ is more sensitive to larger droplet sizes, reflecting their significant contribution to the overall volume distribution [47].

Sample B exhibited the highest droplet size ($p < 0.05$), with droplet size decreasing as the homogenization rates increased. The low homogenization rate of 6500 rpm combined with the short homogenization time of three minutes likely provided insufficient shear force to effectively reduce droplet size. Longer residence times are often necessary when shear force is insufficient to achieve smaller droplet sizes. This finding is corroborated by Alharbi et al. [35], who reported that efficient droplet breakdown depends on both shear speed and residence time. An increase in homogenization rate beyond 9500 rpm resulted in a reduction in $D_{3,2}$ and $D_{4,3}$ values. At the highest homogenization rate (21,500 rpm), the difference between $D_{3,2}$ and $D_{4,3}$ was minimal, indicating a more uniform droplet size distribution compared to the other samples. This observation aligns with the findings by Vargas et al. [48], who observed that higher homogenization rates in a chitosan-oleic acid emulsion produced smaller droplets and more uniform size distributions.

Table 1: Film thickness, volume-surface mean ($D_{3,2}$) and weight mean diameter ($D_{4,3}$) of fish gelatin/cinnamon essential oil films produced using film-forming emulsion (FFE) with various homogenization rates (0, 6500, 9500, 13,500, 17,500, 21,500 rpm)

Homogenization rate (rpm)	Thickness (μm)	$D_{3,2}$ (μm)	$D_{4,3}$ (μm)
A (0)	48.20 ± 3.93^b	4.00 ± 0.46^b	5.89 ± 0.19^{bc}
B (6500)	51.20 ± 4.16^{ab}	4.88 ± 0.79^a	7.46 ± 0.95^a
C (9500)	51.30 ± 2.63^{ab}	4.08 ± 0.16^b	6.25 ± 0.35^b
D (13,500)	54.00 ± 2.79^a	4.05 ± 0.09^b	6.72 ± 0.25^{ab}
E (17,500)	54.90 ± 3.11^a	4.02 ± 0.21^b	6.57 ± 0.83^{ab}
F (21,500)	54.80 ± 2.30^a	3.54 ± 0.13^b	5.11 ± 0.40^c

Note: Means in the same column with different superscript letters are significantly different ($p < 0.05$).

Interestingly, the control samples exhibited $D_{3,2}$ and $D_{4,3}$ values similar ($p \geq 0.05$) to those of the homogenized samples. This similarity may be attributed to the low concentration of CEO, resulting in fewer, sparsely distributed oil droplets within the emulsion. Consequently, the homogenization effect was minimal, as the limited amount of oil present was insufficient to significantly impact droplet size distribution, even with increasing homogenization rates.

3.2 Film Thickness

Table 1 shows the effect of varying homogenization rates on film thickness. The control film (A) exhibited the lowest ($p < 0.05$) thickness, with thickness increasing as homogenization rates increased. This may be attributed to changes in the arrangement of protein molecules in the film matrix. The higher shear forces during homogenization can disrupt the orderly alignment of protein molecules, as lipid droplets become dispersed and embedded within the protein network [49]. This disruption may result in a more protruded film structure, contributing to increased thickness. Additionally, excessive homogenization might have released the emulsifiers from the oil-water interface [39], leading to oil droplet aggregation during the drying process, which further increased the film thickness.

3.3 Mechanical Properties

Emulsion films often demonstrate unique mechanical properties resulting from the presence of dispersed lipid droplets. These properties significantly influence their strength and flexibility, which are essential for preserving product integrity during storage and transportation. The mechanical properties of the films are shown in Table 2. The control film exhibited TS and EAB values of 30 kPa and 144.95%, respectively. The TS and EAB demonstrated a complex, non-linear relationship with homogenization rates. While homogenization did not significantly impact TS ($p \geq 0.05$), a slight increase was observed up to 9500 rpm. The highest ($p < 0.05$) EAB of 165.30% was also achieved at this rate, with EAB declining as homogenization rates further increased. While the highest EAB might suggest plasticizing effect of CEO [12,50,51], this same sample also showed the highest TS, which typically indicates a more rigid structure. This combination could be attributed to the roles of CEO as both a plasticizer and a filler. At this optimal rate (9500 rpm), CEO likely enhances both elasticity and tensile strength by filling spaces within the gelatin matrix, enhancing flexibility while strengthening interchain interactions. Beyond 9500 rpm, the negative impact on TS and EAB likely resulted from CEO aggregation due to the intensive shearing forces, which disrupts matrix continuity and weakens interchain cohesion.

Table 2: Tensile strength (TS), elongation at break (EAB), and water vapor permeability (WVP) of fish gelatin/cinnamon essential oil films produced using film-forming emulsion (FFE) with various homogenization rates (0, 6500, 9500, 13,500, 17,500, 21,500 rpm)

Homogenization rate (rpm)	TS (kPa)	EAB (%)	WVP ($\times 10^{-7}$ g m^{-1} Pa^{-1} s^{-1})
A (0)	30 ± 10^a	144.95 ± 5.90^b	1.53 ± 0.09^b
B (6500)	37 ± 12^a	119.31 ± 8.14^c	1.54 ± 0.08^b
C (9500)	47 ± 6^a	165.30 ± 1.51^a	1.55 ± 0.03^{ab}
D (13,500)	40 ± 10^a	144.91 ± 9.39^b	$1.71 \; 0.10^{ab}$
E (17,500)	33 ± 6^a	144.76 ± 4.12^b	1.80 ± 0.11^{ab}
F (21,500)	27 ± 6^a	135.92 ± 0.92^b	1.96 ± 0.16^a

Note: Means in the same column with different superscript letters are significantly different ($p < 0.05$).

3.4 Water Vapor Permeability

The WVP of biopolymer films is an important factor influencing food quality and shelf life. Low WVP is generally preferred for packaging dried products to prevent moisture absorption, while higher WVP is suitable for fresh produce packaging to prevent condensation. Table 2 shows that WVP in fish gelatin/CEO films slightly ($p \geq 0.05$) increased with higher homogenization rates, increasing from 1.53×10^{-7} g m^{-1} Pa^{-1} s^{-1} in the control to 1.96×10^{-7} g m^{-1} Pa^{-1} s^{-1} at the highest rate (21,500 rpm). This increase in WVP may be due to the CEO droplets within the matrix, which can create free volume, facilitating water molecule movement across the film.

Though smaller lipid droplet sizes are generally expected to enhance water barrier properties by increasing the tortuosity of the matrix [52,53], interactions between the lipid droplets and protein network can also significantly affect WVP. At moderate homogenization rates, CEO droplets likely distribute more evenly, improving the barrier properties. However, the intense shear forces at the highest rate likely led to CEO droplet aggregation, disrupting the protein network and forming a more heterogeneous film structure. This disruption, as also reported by Masamba et al. [54], in a study where homogenization rates of 20,000 rpm resulted in an increase of 152% in WVP in zein films, compared to 10,000 rpm. The results have been attributed to the formation of heterogenous film microstructures which weakens the film matrix, allowing a greater transmission of water vapor molecules [54].

3.5 Light Transmittance and Opacity

Light transmittance and opacity are important optical properties in food packaging materials, as they influence the visual appeal and functional protection of the packaged contents. High transparency is often favored by consumers for clear visibility of the product, while increased opacity can serve to protect the food from potentially harmful UV radiation and photodegradation [55]. Table 3 shows the light transmittance and opacity values for the fish gelatin/CEO films. The control films exhibited light transmittance values of 3.32%, 20.30%, and 25.59% at 200, 280, and 400 nm, respectively, aligning well with the light transmittance values of gelatin film reported previously [7,56,57].

The influence of homogenization rate on light transmittance was minimal across all tested wavelengths ($p \geq 0.05$), likely due to the low CEO concentrations in the films. The fish gelatin/CEO films demonstrated low UV transmittance, particularly at wavelengths of 200 and 280 nm. This reduced transmittance in the UV range can be attributed to the natural UV-absorbing properties of cinnamaldehyde, a major component of CEO, which absorbs at 286 nm [58,59]. Additionally, opacity values remained low and statistically similar ($p \geq 0.05$) across all homogenization rates, as shown in Fig. 2. This consistent low opacity could

be advantageous for packaging applications where moderate UV protection is desired without compromising product visibility.

Table 3: Light transmittance and opacity of fish gelatin/cinnamon essential oil films produced using film-forming emulsion (FFE) with various homogenization rates (0, 6500, 9500, 13,500, 17,500, 21,500 rpm)

Homogenization rate (rpm)	Light transmittance (%) at different wavelength (nm)						Opacity (AU mm^{-1})
	200	280	400	500	600	800	
A (0)	3.32 ± 0.09 [a]	20.30 ± 0.57 [a]	25.59 ± 0.12 [a]	65.64 ± 0.26 [a]	85.80 ± 0.99 [a]	90.59 ± 0.40 [a]	1.38 ± 0.10 [a]
B (6500)	3.33 ± 0.03 [a]	20.22 ± 0.10 [a]	25.54 ± 0.11 [a]	65.42 ± 0.54 [a]	85.15 ± 0.79 [a]	90.60 ± 0.12 [a]	1.36 ± 0.08 [a]
C (9500)	3.42 ± 0.10 [a]	20.33 ± 0.62 [a]	25.63 ± 0.45 [a]	65.38 ± 0.13 [a]	85.58 ± 0.39 [a]	90.47 ± 0.49 [a]	1.32 ± 0.04 [a]
D (13,500)	3.36 ± 0.07 [a]	20.05 ± 0.06 [a]	25.45 ± 0.46 [a]	65.63 ± 0.41 [a]	85.54 ± 0.45 [a]	90.42 ± 0.51 [a]	1.26 ± 0.04 [a]
E (17,500)	3.43 ± 0.09 [a]	20.63 ± 0.29 [a]	25.53 ± 0.10 [a]	65.77 ± 0.06 [a]	85.94 ± 0.10 [a]	90.57 ± 0.31 [a]	1.20 ± 0.01 [a]
F (21,500)	3.40 ± 0.16 [a]	20.13 ± 0.09 [a]	25.59 ± 0.06 [a]	65.55 ± 0.48 [a]	85.36 ± 0.42 [a]	90.42 ± 0.11 [a]	1.25 ± 0.04 [a]

Note: Means in the same column with different superscript letters are significantly different ($p < 0.05$).
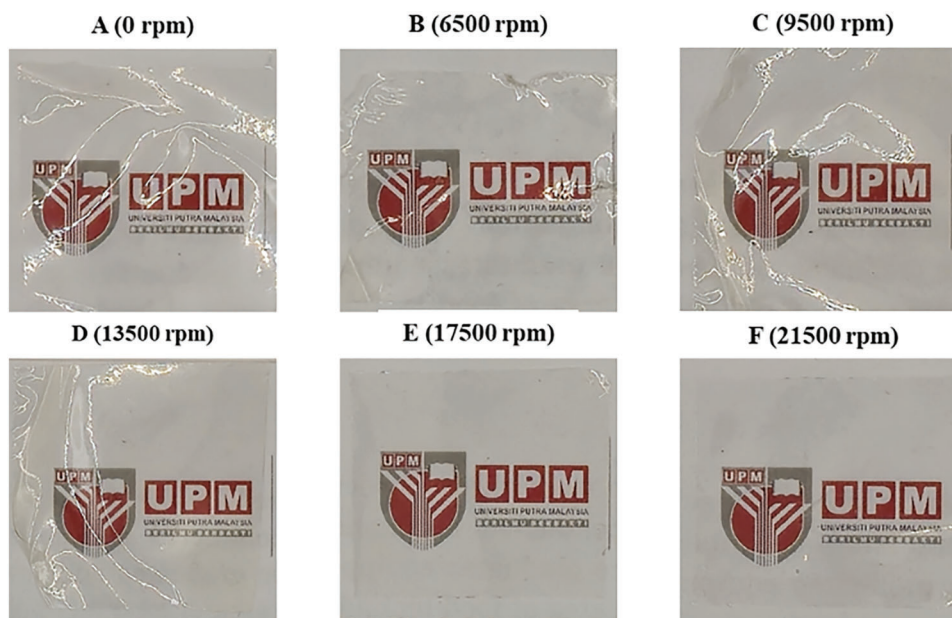

Figure 2: Appearance of fish gelatin films incorporated with cinnamon essential oil produced using film-forming emulsion (FFE) with various homogenization rates (0, 6500, 9500, 13,500, 17,500, 21,500 rpm)

3.6 Surface Microstructure (SEM and CLSM)

Fig. 3 shows the scanning electron microscopy (SEM) images of fish gelatin/CEO films, prepared at different homogenization rates. The surface microstructures of these films were noticeably affected by the homogenization rates. The control film exhibited a dense and slightly rough structure, likely due to the presence of oil in the gelatin matrix. Similar findings have been reported previously, where the incorporation of palm wax into gelatin produced a rougher surface compared to pure gelatin films [60].

However, when the homogenization rate exceeded 13,500 rpm, the films developed irregular surface microstructures with visible clumps, likely caused by oil droplets disrupting the film surface. The high shear rates may have caused the aggregation of lipid droplets, reducing film stability [39], and forcing oil droplets out during the drying process. Since smaller droplet sizes were achieved at higher

homogenization rates, as indicated in Table 1, it is likely that the aggregation of the CEO occurred during the film drying process. Similar results have been reported in a previous study [54], where increasing the homogenization rate from 10,000 to 20,000 rpm resulted in a coarse and heterogeneous microstructure in zein-oleic acid composite films.
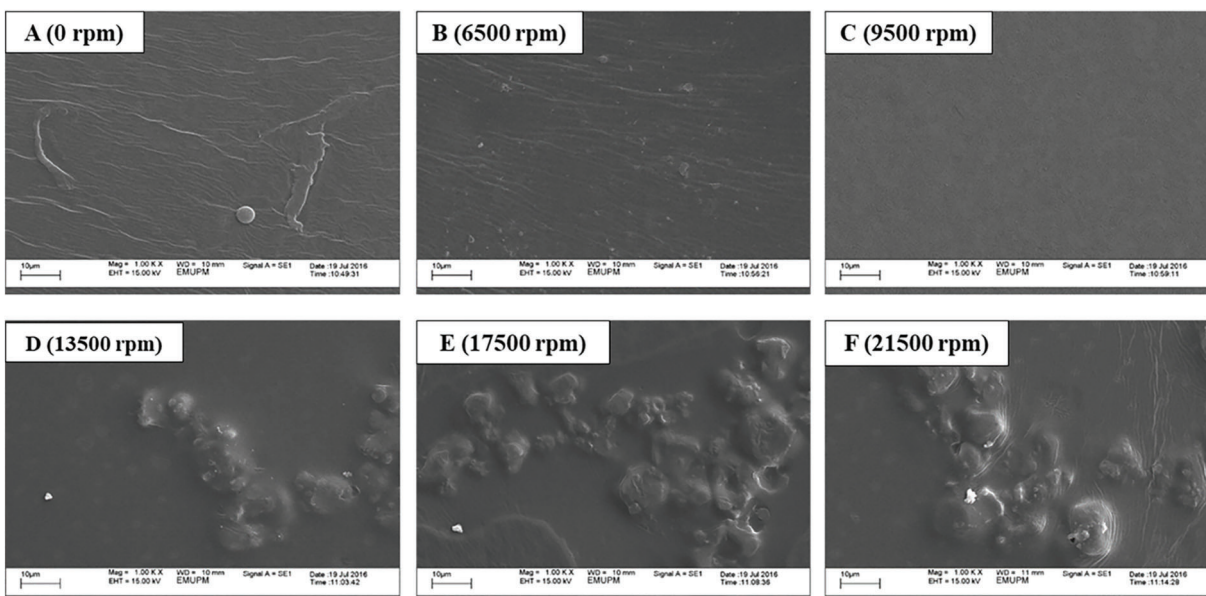

Figure 3: SEM surface microstructure of fish gelatin films incorporated with cinnamon essential oil produced using film-forming emulsion (FFE) with various homogenization rates (0, 6500, 9500, 13,500, 17,500, 21,500 rpm)

At 21,500 rpm, microscopic pores were visible on the film surface, likely contributing to the significantly ($p < 0.05$) higher WVP compared to the other samples. Likewise, in a study by Almasi et al. [61], microemulsion films of calcium alginate and thyme essential oil exhibited high porosity, which resulted in elevated WVP.

Fig. 4 shows the CLSM images of the films. The red areas in the images represent the distribution of CEO within the gelatin matrix. In the control film (A), the essential oil was dispersed throughout the continuous gelatin phase, with lipid droplets exhibiting inconsistent sizes. At 9500 rpm, the oil droplets appeared to be homogeneously distributed, with more uniformly sized lipid droplets evenly dispersed within the gelatin matrix. This uniform distribution likely contributed to the enhanced mechanical properties observed at this homogenization rate.

3.7 Surface Topography

Fig. 5 shows the surface topographies of fish gelatin/CEO films at different homogenization rates. The corresponding roughness parameters, R_a and R_q, measured by AFM, are presented in Table 4. All the films share similar ($p \geq 0.05$) R_a and R_q, regardless of the homogenization rate. Among the films, the control film (A) exhibited the highest R_a and R_q values, at 13.38 and 19.04 nm, respectively. The higher roughness may be attributed to the immiscibility between the hydrophilic gelatin and hydrophobic CEO, exacerbated by the inconsistent lipid droplet sizes, as observed in the CLSM images. Film C, produced at 9500 rpm, showed lower surface roughness, aligning with the SEM results, where the film displayed a smooth and homogeneous microstructure. This lower roughness likely reflects the uniform distribution of CEO droplets within the gelatin matrix.
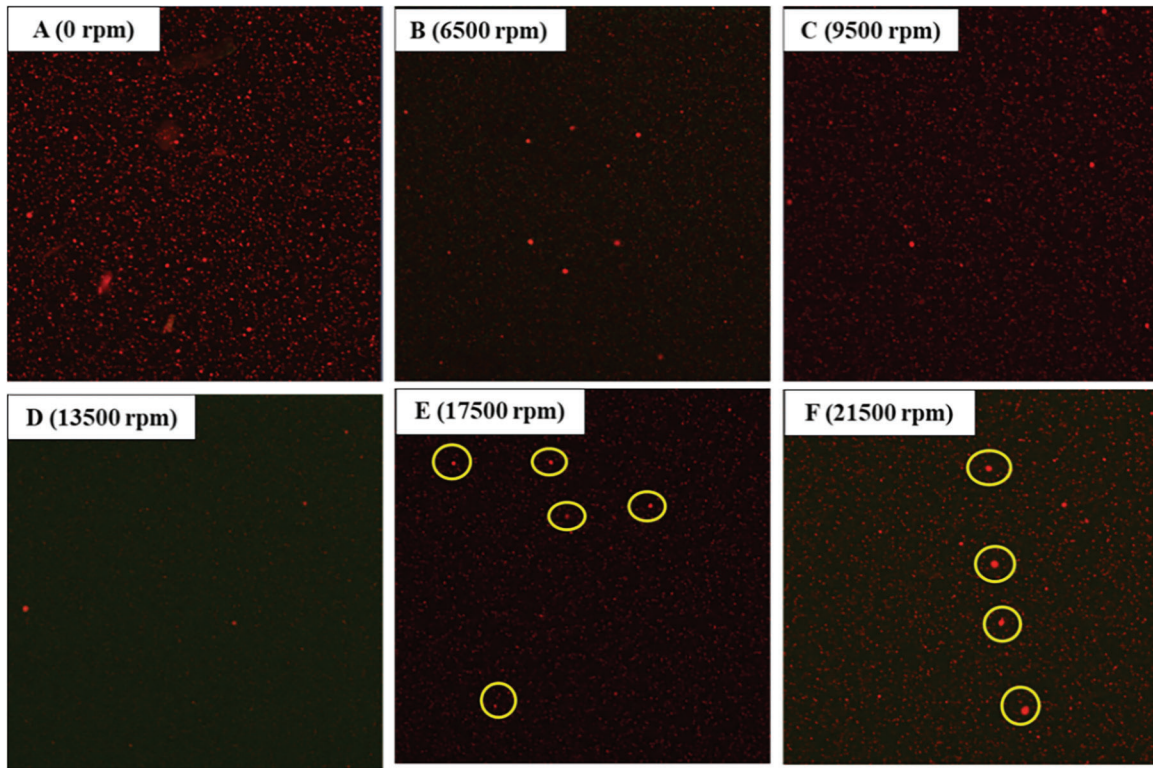
Figure 4: Confocal laser scanning micrographs of fish gelatin films incorporated with cinnamon essential oil produced using film-forming emulsion (FFE) with various homogenization rates (0, 6500, 9500, 13,500, 17,500, 21,500 rpm)
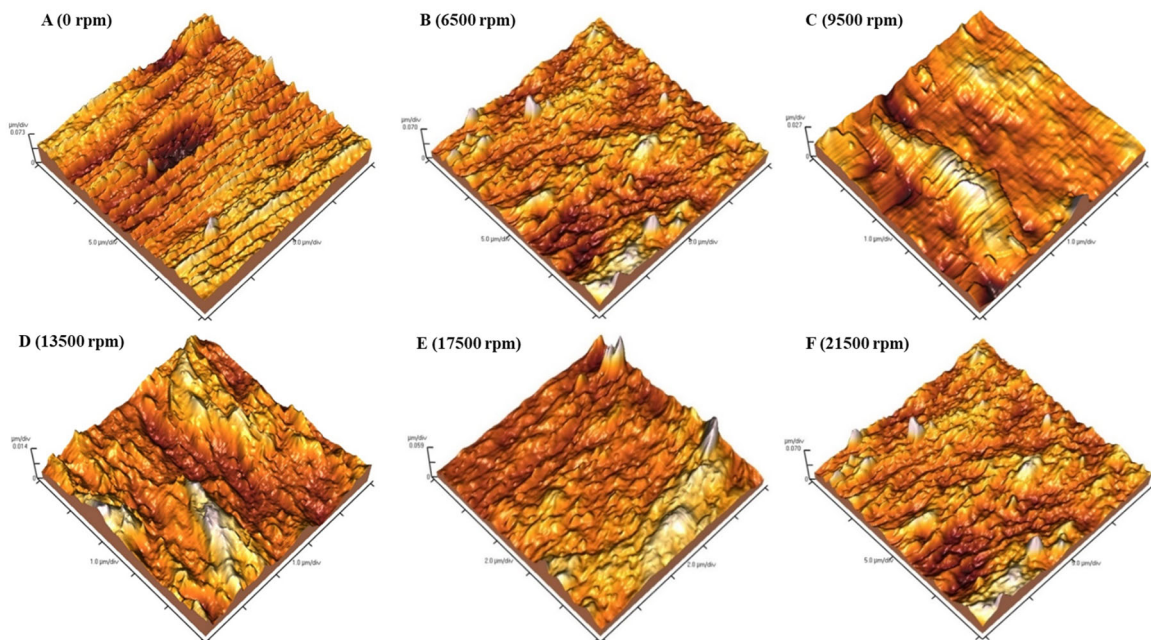

Figure 5: AFM images of fish gelatin films incorporated with cinnamon essential oil produced using film-forming emulsion (FFE) with various homogenization rates (0, 6500, 9500, 13,500, 17,500, 21,500 rpm)

Table 4: Average roughness (R_a) and root mean square roughness (R_q) of fish gelatin/cinnamon essential oil films produced using film-forming emulsion (FFE) with various homogenization rates (0, 6500, 9500, 13,500, 17,500, 21,500 rpm)

Homogenization rate (rpm)	R_a (nm)	R_q (nm)
A (0)	13.38 ± 0.97^a	19.04 ± 1.24^a
B (6500)	8.37 ± 2.64^a	10.99 ± 3.67^a
C (9500)	4.91 ± 1.53^a	6.46 ± 2.23^a
D (13,500)	7.52 ± 4.88^a	9.11 ± 5.71^a
E (17,500)	7.61 ± 0.56^a	9.08 ± 0.45^a
F (21,500)	10.40 ± 2.64^a	13.11 ± 3.76^a

Note: Means in the same column with different superscript letters are significantly different ($p < 0.05$).

As the homogenization rate increased, the roughness values of the films C to F showed an increasing trend. The R_a values increased from 4.91 to 10.40 nm, while the R_q values increased from 6.46 to 13.11 nm. The R_q value, which gives more weight to larger peaks and valleys, is considered a better measure of surface irregularities [62]. The higher R_q values compared to R_a value supported the AFM observations, where occasional sharp peaks were visible on the film surfaces.

This increased roughness may be attributed to the entrapment of large CEO droplets in the film matrix or interactions between the oil molecules and gelatin chains that affect chain entanglements [63], suggesting that higher homogenization rates reduced emulsion stability during the drying process. Moreover, the increased surface tension between the oil and water phases, due to the presence of smaller oil droplets, may contribute to a rougher film morphology, as observed in a previous study [64]. The CEO droplets likely underwent agglomeration during drying, leading to surface roughness and irregularities, as also observed in the SEM images.

4 Conclusion

This study investigates the impact of homogenization rates on the physical and barrier properties of fish gelatin films containing cinnamon essential oil (CEO). The findings indicate that as the homogenization rate increased, droplet size and distribution in the film-forming emulsion (FFE) became significantly smaller and narrower. An optimal homogenization rate of 9500 rpm enhanced film flexibility and smoothness, likely due to a well-distributed CEO phase within the gelatin matrix. However, homogenization rates above 17,500 rpm led to CEO droplet aggregation, which disrupted the film matrix and increased water vapor permeability. These results contribute to the development of sustainable active packaging materials by demonstrating that adjusting homogenization rates can effectively tailor the mechanical and barrier properties of essential oil-enriched gelatin films. A limitation of this study is the focus on a single essential oil and specific homogenization parameters, which may not capture the broader behavior of other bioactive compounds or processing conditions. Future studies could explore a wider range of bioactive compounds and process variables for broader applicability. Additionally, the improvement of mechanical strength and water vapor barrier of the should also be studied. Such advancements can benefit the packaging industry by extending the shelf life of specific food products, particularly those requiring high moisture barriers.

Author Contributions: The authors confirm contribution to the paper as follows: study conception and design: Nur Hanani Z. A.; data collection: See Cheng Lee; analysis and interpretation of results: See Cheng Lee, Han Lyn Foong; draft manuscript preparation: Han Lyn Foong. All authors reviewed the results and approved the final version of the manuscript.

Availability of Data and Materials: Data available on request from the authors.

Ethics Approval: Not applicable.

Conflicts of Interest: The authors declare no conflicts of interest to report regarding the present study.

References

1. Tagrida M, Nilsuwan K, Gulzar S, Prodpran T, Benjakul S. Fish gelatin/chitosan blend films incorporated with betel (*Piper betle* L.) leaf ethanolic extracts: characteristics, antioxidant and antimicrobial properties. Food Hydrocoll. 2023 Apr 1;137.

2. Mirpoor SF, Corrado I, Di Girolamo R, Dal Poggetto G, Panzella L, Borselleca E, et al. Manufacture of active multilayer films made of functionalized pectin coated by polyhydroxyalkanoates: a fully renewable approach to active food packaging. Polymer. 2023 Jul 18;281:126136. doi:10.1016/j.polymer.2023.126136.

3. Mortalò C, Russo P, Miorin E, Zin V, Paradisi E, Leonelli C. Extruded composite films based on polylactic acid and sodium alginate. Polymer. 2023 Aug 8;282:126162. doi:10.1016/j.polymer.2023.126162.

4. Tagrida M, Gulzar S, Nilsuwan K, Prodpan T, Zhang B, Benjakul S. Polylactic acid film coated with electrospun gelatin/chitosan nanofibers containing betel leaf ethanolic extract: properties, bioactivities, and use for shelf-life extension of tilapia slices. Molecules. 2022;27:5877. doi:10.3390/molecules27185877.

5. Kim HJ, Roy S, Rhim JW. Gelatin/agar-based color-indicator film integrated with *Clitoria ternatea* flower anthocyanin and zinc oxide nanoparticles for monitoring freshness of shrimp. Food Hydrocoll. 2022;124(4):107294. doi:10.1016/j.foodhyd.2021.107294.

6. Vargas-Torrico MF, Aguilar-Méndez MA, Ronquillo-de Jesús E, Jaime-Fonseca MR, von Borries-Medrano E. Preparation and characterization of gelatin-carboxymethylcellulose active film incorporated with pomegranate (*Punica granatum* L.) peel extract for the preservation of raspberry fruit. Food Hydrocoll. 2024 May 1;150:109677. doi:10.1016/j.foodhyd.2023.109677.

7. Chen L, Gao J, Zhang X, Li J, Zhang Y, Qiang T. Octadecylamine modified gelatin-based biodegradable packaging film with good water repellency and improved moisture service reliability. Int J Biol Macromol. 2024 Nov 1;279:135218. doi:10.1016/j.ijbiomac.2024.135218.

8. Zheng H, Chen X, Li L, Qi D, Wang J, Lou J, et al. Development of gelatin-based active packaging and its application in bread preservation. J Renew Mater. 2023;11(10):3693–709. doi:10.32604/jrm.2023.027748.

9. Nur Hanani ZA, Cheng Yee F, Nor-Khaizura MAR. Effect of pomegranate (*Punica granatum* L.) peel powder on the antioxidant and antimicrobial properties of fish gelatin films as active packaging. Food Hydrocoll. 2019;89(1):253–9. doi:10.1016/j.foodhyd.2018.10.007.

10. Chen L, Qiang T, Ren W, Tian Q, Zhang X, Zhang HJ. Strong, water-repellent, and recyclable gelatin-based bioplastic film as sustainable express packaging film. J Clean Prod. 2023 Jan 20;385:135705. doi:10.1016/j.jclepro.2022.135705.

11. Nor Adilah A, Gun Hean C, Nur Hanani ZA. Incorporation of graphene oxide to enhance fish gelatin as bio-packaging material. Food Packag Shelf Life. 2021;28(48):100679. doi:10.1016/j.fpsl.2021.100679.

12. Tügen A, Ocak B, Özdestan-Ocak Ö. Development of gelatin/chitosan film incorporated with lemon essential oil with antioxidant properties. J Food Meas Charact. 2020;14(6):3010–9. doi:10.1007/s11694-020-00547-5.

13. Nurul Syahida S, Ainun ZMA, Ismail-Fitry MR, Nur Hanani ZA. Development and characterisation of gelatine/palm wax/lemongrass essential oil (GPL)-coated paper for active food packaging. Packag Technol Sci. 2020;33(10):417–31. doi:10.1002/pts.2512.

14. Kim H, Beak SE, Song KB. Development of a hagfish skin gelatin film containing cinnamon bark essential oil. LWT. 2018;96:583–8. doi:10.1016/j.lwt.2018.06.016.

15. Lucas-González R, Yilmaz B, Mousavi Khaneghah A, Hano C, Shariati MA, Bangar SP, et al. Cinnamon: An antimicrobial ingredient for active packaging. Food Packag Shelf Life. 2023 Mar 1;35:101026. doi:10.1016/j.fpsl.2023.101026.

16. Lim ZQJ, Tong SY, Wang K, Lim PN, Thian ES. Cinnamon oil incorporated polymeric films for active food packaging. Mater Lett. 2022 Apr 15;313:131744. doi:10.1016/j.matlet.2022.131744.

17. Anuar H, Nur Fatin Izzati AB, Sharifah Nurul Inani SM, Siti Nur E'zzati MA, Siti Munirah Salimah AB, Ali FB, et al. Impregnation of cinnamon essential oil into plasticised polylactic acid biocomposite film for active food packaging. J Packag Technol Res. 2017 Oct;1(3):149–56. doi:10.1007/s41783-017-0022-1.

18. Kang JH, Song KB. Characterization of Job's tears (*Coix lachryma-jobi* L.) starch films incorporated with clove bud essential oil and their antioxidant effects on pork belly during storage. LWT. 2019 Aug 1;111:711–8. doi:10.1016/j.lwt.2019.05.102.

19. Wang Y, Du YT, Xue WY, Wang L, Li R, Jiang ZT, et al. Enhanced preservation effects of clove (*Syzygium aromaticum*) essential oil on the processing of Chinese bacon (preserved meat products) by beta cyclodextrin metal organic frameworks (β-CD-MOFs). Meat Sci. 2023;195(4):108998. doi:10.1016/j.meatsci.2022.108998.

20. Poongavanam SS, Subramaniyan V, Rajendra AB, Sellamuthu PS, Jarugala J, Sadiku ER. Physiochemical analysis of *Manilkara zapota* (Sapota) coated with aloe vera gel and enriched with ajwain and oregano essential oils. Coatings. 2023 Aug 1;13(8):1358. doi:10.3390/coatings13081358.

21. Criollo-Feijoo J, Salas-Gomez V, Cornejo F, Auras R, Salazar R. Cassava bagasse starch and oregano essential oil as a potential active food packaging material: a physicochemical, thermal, mechanical, antioxidant, and antimicrobial study. Heliyon. 2024 Aug 30;10(16):e36150. doi:10.1016/j.heliyon.2024.e36150.

22. Li YX, Erhunmwunsee F, Liu M, Yang K, Zheng W, Tian J. Antimicrobial mechanisms of spice essential oils and application in food industry. Food Chem. 2022 Jul 15;382:132312. doi:10.1016/j.foodchem.2022.132312.

23. Lv H, Huo S, Zhao L, Zhang H, Liu Y, Liu S, et al. Preparation and application of cinnamon-Litsea cubeba compound essential oil microcapsules for peanut kernel postharvest storage. Food Chem. 2023 Jul 30;415:135734. doi:10.1016/j.foodchem.2023.135734.

24. Goel B, Mishra S. Medicinal and nutritional perspective of cinnamon: a mini-review. European J Med Plants. 2020 Feb 27;31(3):10–6.

25. Błaszczyk N, Rosiak A, Kałużna-Czaplińska J. The potential role of cinnamon in human health. Forests. 2021;12(5):648. doi:10.3390/f12050648.

26. Tian Y, Lei Q, Yang F, Xie J, Chen C. Development of cinnamon essential oil-loaded PBAT/thermoplastic starch active packaging films with different release behavior and antimicrobial activity. Int J Biol Macromol. 2024 Apr 1;263:130048. doi:10.1016/j.ijbiomac.2024.130048.

27. Nirmal NP, Chunhavacharatorn P, Chandra Khanashyam A, Li L, Al-Asmari F. Cinnamon bark oil in water nanoemulsion formulation, characterization, and antimicrobial activities. LWT. 2023 Apr 1;179:114671. doi:10.1016/j.lwt.2023.114671.

28. Siew ZZ, Chan EWC, Wong CW. Hydrophobic bioactive constituents of cinnamon bark as inhibitor of polyphenol oxidase from Musa acuminata 'Mas' peel. Biocatal Agric Biotechnol. 2022;45(4):102504. doi:10.1016/j.bcab.2022.102504.

29. de Carvalho APA, Conte Junior CA. Green strategies for active food packagings: a systematic review on active properties of graphene-based nanomaterials and biodegradable polymers. Trends Food Sci Technol. 2020;103(12):130–43. doi:10.1016/j.tifs.2020.07.012.

30. Das PP, Prathapan R, Ng KW. Advances in biomaterials based food packaging systems: current status and the way forward. Biomater Adv. 2024 Nov 1;164:213988. doi:10.1016/j.bioadv.2024.213988.

31. Liu X, Jia J, Duan S, Zhou X, Xiang A, Lian Z, et al. Zein/MCM-41 nanocomposite film incorporated with cinnamon essential oil loaded by modified supercritical CO_2 impregnation for long-term antibacterial packaging. Pharmaceutics. 2020;12(169):1–12.

32. Hassanshahi N, Hu G, Lee K, Li J. Effect of ultrasonic homogenization on crude oil-water emulsion stability. J Environ Sci Health Part A. 2023 Feb 23;58(3):211–21. doi:10.1080/10934529.2023.2178788.

33. Wigati LP, Wardana AA, Jothi JS, Leonard S, Van TT, Yan X, et al. Preserving mandarin quality during ambient storage using edible coatings of pregelatinized corn starch pickering emulsions and essential oil. Food Biosci. 2023 Jun 1;53:102710. doi:10.1016/j.fbio.2023.102710.

34. Kupikowska-Stobba B, Domagała J, Kasprzak MM. Critical review of techniques for food emulsion characterization. Appl Sci. 2024 ;14(3):1069. doi:10.3390/app14031069.

35. G.Alharbi G, Abdulhamid MA. Optimization of water/oil emulsion preparation: impact of time, speed, and homogenizer type on droplet size and dehydration efficiency. Chemosphere. 2023 Sep 1;335:139136. doi:10.1016/j.chemosphere.2023.139136.

36. Chu Y, Cheng W, Feng X, Gao C, Wu D, Meng L, et al. Fabrication, structure and properties of pullulan-based active films incorporated with ultrasound-assisted cinnamon essential oil nanoemulsions. Food Packag Shelf Life. 2020 Sep 1;25:100547. doi:10.1016/j.fpsl.2020.100547.

37. Gazolu-Rusanova D, Lesov I, Tcholakova S, Denkov N, Ahtchi B. Food grade nanoemulsions preparation by rotor-stator homogenization. Food Hydrocoll. 2020 May 1;102:105579. doi:10.1016/j.foodhyd.2019.105579.

38. Rosdi MRH, Ariffin A, Ishak ZAM. Optimizing homogenization parameters for improving ethylene vinyl acetate emulsion stability in pour point depressant application. J King Saud Univ-Eng Sci. 2018 Apr 1;30(2):105–15.

39. Hao X, Elakneswaran Y, Shimokawara M, Kato Y, Kitamura R, Hiroyoshi N. Impact of the temperature, homogenization condition, and oil property on the formation and stability of crude oil emulsion. Energy Fuels. 2024 Jan 18;38(2):979–94. doi:10.1021/acs.energyfuels.3c04034.

40. Salum P, Ulubaş Ç, Güven O, Cam M, Aydemir LY, Erbay Z. The impact of homogenization techniques and conditions on water-in-oil emulsions for casein hydrolysate-loaded double emulsions: a comparative study. Food Sci Nutr. 2024 Oct 18;12(11):9585–99. doi:10.1002/fsn3.v12.11.

41. Bergslien E. Gems and gemstones: those most precious of all minerals. In: An introduction to forensic geoscience. Hoboken, NJ, USA: Wiley-Blackwell; 2012. p. 168–219.

42. ASTM. D 882-02: standard test method for tensile properties of thin plastic sheeting. In: Annual book of ASTM standards. Philadelphia, PA, USA: ASTM International; 2002. p. 1–10.

43. ASTM. E 96-95: standard test methods for water vapor transmission of materials. In: Annual book of ASTM standards. Philadelphia, PA, USA: ASTM International; 1995. p. 1–8.

44. Han Lyn F, Chin Ping T, Zawawi RM, Nur Hanani ZA. Physicochemical properties of chitosan/graphene oxide composite films and their effects on storage stability of palm-oil based margarine. Food Hydrocoll. 2021;117:106707. doi:10.1016/j.foodhyd.2021.106707.

45. Wexler A. Vapor pressure equation for water in range 3 to 100 degrees C. J Res Natl Bur Stand A Phys Chem. 1976;80A(3):775–85.

46. Auty MAE, Twomey M, Guinee TP, Mulvihill DM. Development and application of confocal scanning laser microscopy methods for studying the distribution of fat and protein in selected dairy products. J Dairy Res. 2001;68(3):417–27. doi:10.1017/S0022029901004873.

47. Lefroy KS, Murray BS, Ries ME. Relationship between size and cellulose content of cellulose microgels (CMGs) and their water-in-oil emulsifying capacity. Colloids Surf A Physicochem Eng Asp. 2022 Aug 20;647:128926. doi:10.1016/j.colsurfa.2022.128926.

48. Vargas M, Perdones Á, Chiralt A, Cháfer M, González-Martínez C. Effect of homogenization conditions on physicochemical properties of chitosan-based film-forming dispersions and films. Food Hydrocoll. 2011 Jul 1;25(5):1158–64. doi:10.1016/j.foodhyd.2010.11.002.

49. Tongnuanchan P, Benjakul S, Prodpran T, Pisuchpen S, Osako K. Mechanical, thermal and heat sealing properties of fish skin gelatin film containing palm oil and basil essential oil with different surfactants. Food Hydrocoll. 2016 May 1;56:93–107. doi:10.1016/j.foodhyd.2015.12.005.

50. Yanwong S, Threepopnatkul P. Effect of peppermint and citronella essential oils on properties of fish skin gelatin edible films. IOP Conf Ser: Mater Sci Eng. 2015;87(1):012064.

51. Laorenza Y, Harnkarnsujarit N. Ginger oil and lime peel oil loaded PBAT/PLA via cast-extrusion as shrimp active packaging: microbial and melanosis inhibition. Food Packag Shelf Life. 2023 Sep 1;38:101116. doi:10.1016/j.fpsl.2023.101116.

52. Fabra MJ, Pérez-Masiá R, Talens P, Chiralt A. Influence of the homogenization conditions and lipid self-association on properties of sodium caseinate based films containing oleic and stearic acids. Food Hydrocoll. 2011 Jul 1;25(5):1112–21. doi:10.1016/j.foodhyd.2010.10.008.

53. Tabatabaei SD, Ghiasi F, Hashemi Gahruie H, Hosseini SMH. Effect of emulsified oil droplets and glycerol content on the physicochemical properties of Persian gum-based edible films. Polym Test. 2022 Feb 1;106(3):107427. doi:10.1016/j.polymertesting.2021.107427.

54. Masamba K, Li Y, Zhong F. Effect of homogenization stirring speed on mechanical and water barrier properties of gallic acid treated zein-oleic acid composite films. Food Packag Shelf Life. 2016 Dec 1;10:97–105. doi:10.1016/j.fpsl.2016.10.006.

55. Roy S, Ramakrishnan R, Goksen G, Singh S, Łopusiewicz Ł. Recent progress on UV-light barrier food packaging films—a systematic review. Innov Food Sci Emerg Technol. 2024 Jan 1;91:103550. doi:10.1016/j.ifset.2023.103550.

56. Wang X, Liu B, Hayat K, Xia S, Cui H, Yu J. Fabrication and characterization of long-lasting antifungal film containing cinnamaldehyde-loaded complex coacervation microcapsules based on gelatin and gum Arabic. Int J Biol Macromol. 2024 Nov 1;281:136603. doi:10.1016/j.ijbiomac.2024.136603.

57. Didar Z. Investigating the mechanical, physical and antimicrobial properties of gelatin films containing Cinnamomum verum hydrosol. J Food Bioprocess Eng. 2019;2(2):113–8.

58. Pan MB, Hughes CS, Lynch HN, Schilling MM, Liyana Pathiranage A. Investigation of cinnamaldehyde derivatives as potential organic UV filters. J Chem. 2022;2022(9):1–7. doi:10.1155/2022/7010428.

59. Abdul Hakeem Memon P, Laghari M, Ur Rehman Mughal U, LAL Maheshwari M. Spectrophotometric determination of cinnamaldehyde from crude drugs and herbal preparations. Artic Asian J Chem. 2011;23(2):631–5.

60. Syahida N, Fitry I, Zuriyati A, Hanani N. Effects of palm wax on the physical, mechanical and water barrier properties of fish gelatin films for food packaging application. Food Packag Shelf Life. 2020;23(1):100437. doi:10.1016/j.fpsl.2019.100437.

61. Almasi L, Radi M, Amiri S, McClements DJ. Fabrication and characterization of antimicrobial biopolymer films containing essential oil-loaded microemulsions or nanoemulsions. Food Hydrocoll. 2021 Aug 1;117(1):106733. doi:10.1016/j.foodhyd.2021.106733.

62. Hendaoui A. Low solar absorptance, high emittance performance thermochromic VO_2-based smart radiator device. Nanomater. 2022 Dec 1;12(24):4422. doi:10.3390/nano12244422.

63. Karami N, Kamkar A, Shahbazi Y, Misaghi A. Electrospinning of double-layer chitosan-flaxseed mucilage nanofibers for sustained release of Ziziphora clinopodioides essential oil and sesame oil. LWT. 2021 Apr 1;140:110812. doi:10.1016/j.lwt.2020.110812.

64. Shahbazi Y, Shavisi N, Karami N, Lorestani R, Dabirian F. Electrospun carboxymethyl cellulose-gelatin nanofibrous films encapsulated with *Mentha longifolia* L. essential oil for active packaging of peeled giant freshwater prawn. LWT. 2021 Dec 1;152:112322. doi:10.1016/j.lwt.2021.112322.